Polymers for Advanced Technologies

WILEY

polymers advanced technologies

RESEARCH ARTICLE

Polymeric Modulation of Natural Microcapsules: A Multimodal Platform for Enhanced Mucoadhesion and Site-Specific Oral Drug Delivery

Volkan Aylanc[1,2,3] | Seymanur Ertosun[1,2] | Nuno Vale[3,4,5] | Cristina Freire[2] | Miguel Vilas-Boas[1]

[1]CIMO, LA SusTEC, Instituto Politécnico de Bragança, Campus de Santa Apolónia, Bragança, Portugal | [2]LAQV-REQUIMTE, Departamento de Química e Bioquímica, Faculdade de Ciências, Universidade do Porto, Porto, Portugal | [3]PerMed Research Group, Center for Health Technology and Services Research (CINTESIS), Porto, Portugal | [4]CINTESIS@RISE, Faculty of Medicine, University of Porto, Porto, Portugal | [5]Department of Community Medicine, Health Information and Decision (MEDCIDS), Faculty of Medicine, University of Porto, Porto, Portugal

Correspondence: Volkan Aylanc (volkan@ipb.pt) | Miguel Vilas-Boas (mvboas@ipb.pt)

Received: 6 March 2026 | **Revised:** 2 May 2026 | **Accepted:** 5 May 2026

Keywords: bee pollen | controlled delivery | mucoadhesion enhancement biocompatibility | polymer coating | sporopollenin-based carriers

ABSTRACT

Sporopollenin, a highly robust, biocompatible, and chemically resistant biopolymer derived from pollen grains, represents an underexploited renewable resource for sustainable pharmaceutical applications. Therewith, the broader application of oral pollen-based systems is restricted by morphology-related limitations, premature gastric release, and insufficient intestinal adhesion. Herein, sporopollenin microcapsules (SMCs) were produced from *Castanea* sp. (Cas) and *Helianthus* sp. (Hel) bee pollen using a solvent-efficient, scalable purification strategy. The microcapsules were then surface-functionalized via a clean photochemical approach to enhance mucoadhesion and coated with either biodegradable alginate (Alg) or pH-responsive eudragit (Eud), modulating the controlled intestinal release of the model drug 5-Fluorouracil (5-FU). Scanning electron microscope (SEM), confocal laser scanning microscopy (CLSM), and laser diffraction particle analysis confirmed successful purification, with average sizes of 11.2 μm (Cas) and 24.1 μm (Hel). Drug loading capacities were 29% and 36%, respectively, and Fourier-transform infrared (FTIR) and thermogravimetric analysis (TGA) validated successful encapsulation. Uncoated SMCs released 63%–73% of 5-FU within 1 h, whereas Alg or Eud coatings delayed release, achieving sustained, super case-II transport profiles. Bioadhesion testing showed Hel-SMCs had a higher work of adhesion (0.298 mJ/cm^2) than Cas-SMCs (0.079 mJ/cm^2), supporting prolonged residence in the target site. Biocompatibility assays of SMCs in Vero cells indicated no cytotoxic effects, $GI_{50} > 700$ μg/mL. Overall, polymer-coated SMCs demonstrate strong potential as sustainable oral drug delivery systems, integrating effective encapsulation, controlled and mucoadhesive release behavior with multifunctional, low-waste design principles that advance sustainable pharmacy and resource efficiency.

1 | Introduction

The development of micro- and nano-sized drug delivery systems has become increasingly important for optimizing therapeutic efficacy through improved drug protection, controlled release, and enhanced interaction with biological tissues [1–3]. Among these systems, naturally derived biopolymers such as chitosan, alginate, and gelatin have been widely explored due to their biocompatibility, biodegradability, and versatile functional properties in drug delivery applications [4]. Pollen grains, with their microscale dimensions and nanoscale pores, are potential candidates for drug loading and controlled release. Pollen grains are male gametophytes that ensure the continuation of the life cycle of land plants [5]. Ranging in

size from a few micrometers to tens of micrometers, pollen protects fertile cell material from external factors, including ultraviolet (UV) radiation, extreme temperature fluctuations, and other chemical and physical disturbances [6]. A typical pollen grain is a microstructure resembling a natural capsule, with an outer shell composed of the biopolymer sporopollenin and an inner shell of cellulose and pectin [7]. The relatively inert and resilient nature of sporopollenin displays a wide range of complex supramolecular structures, along with varying sizes, shapes, and porosities [8]. As a result, sporopollenin is one of the most durable and resistant materials of biological origin, capable of withstanding various mechanical impacts and organic solvents [9–11]. These properties have enabled the successful use of natural sporopollenin in removing heavy metals, serving as catalyst solid supports, medical imaging, and encapsulating enzymes, drugs, bioactive compounds, and living cells [6, 8, 12].

This feature of the pollen wall allows for the fabrication of solid oral dosage forms, providing a highly reproducible and convenient method of drug delivery [13, 14]. These formulations are generally easy to manufacture and stable, making them a common form of self-medication. They are also suitable for controlled and extended-release oral therapeutic delivery [15]. Moreover, designing efficient delivery systems should ensure that the active pharmaceutical ingredient reaches the desired environment while maintaining its bioactivity, which enhances absorption and reduces the risk of dose dumping [6, 14]. SMCs purified from specific pollen grains have already been explored as solid oral dosage forms for the release and control of active compounds in the gastrointestinal tract, due to their structural integrity, biocompatibility, and non-toxicity [16–19]. However, the pores (known as apertures) in the pollen wall, which can range from hundreds of nanometers to a few micrometers, and the nanochannels along the pollen wall facilitate the loading of encapsulated material but, at the same time, can also cause rapid discharge of loaded material in the release medium [20]. Attempts have been made to attenuate this handicap by coating the outer surface of microcapsules with Alg coating [7, 15], enteric coating [16, 21], and chitosan coating cross-linked with glutaraldehyde [18], or depositing a polymer on the SMCs' inner surface [19]. These strategies have been largely effective in preventing premature drug release during the gastric phase, although to varying extents. Notably, the SMCs used in these studies were generally derived from pollen types lacking multiple surface pores.

Given the structural diversity among pollen types, it is important to investigate how SMCs obtained from pollen with natural apertures respond to polymer coating strategies, in order to broaden the applicability of pollen-derived microcapsules in drug delivery. To do so, there are several desirable properties that must be considered during formulation development: SMCs should protect orally administered encapsulated therapeutic molecules throughout their journey until they are delivered to the desired site. This is crucial because the ingress of gastric fluid and enzymatic degradation can denature the molecules and affect their activity [7]; prevention of premature release and maximizing the delivery and controlled release of the therapeutic dose in the target tissue, for example, the small intestine or colon [15, 16]. Moreover, the uniform distribution, number of apertures, and structure of SMCs can play a crucial role in encapsulation efficiency and release rate, which is essential in the design of oral therapeutics [7, 10]. Our previous study with various pollen types has demonstrated that smaller SMCs exhibit a faster release behavior [20]. In contrast, larger SMCs released their contents over a longer period due to an extended diffusion pathway and a reduced interfacial area, considering the surface ration area-to volume, between the SMCs and the release medium [20, 22]. Building on these findings, here we investigated the pollen species Cas and Hel, which share the same pore number and structural characteristics but differ in volume. This volume difference enables us to tailor the site of release by leveraging the impact of SMC's surface morphology on its release performance. Moreover, we also evaluated the mucoadhesive properties of the developed SMCs, in contact with biological tissues, to better understand their ability for prolonged gastrointestinal residence. This is a critical feature for oral microcapsules, since stronger bioadhesiveness properties enhance the residence time of SMCs at the target site, improving precision delivery and drug absorption [23].

Here, we aimed to develop a strategy for transporting 5-FU, used as a model drug, entrapped within pollen microcarriers, to be released in the small intestine or colon, thereby protecting it from gastric degradation and premature release. Typically, SMCs exhibit hydrophobic behavior, so we treated them with UV irradiation to enhance their affinity toward aqueous environments, rendering them super hydrophilic. This modification was also key for improving the encapsulation efficiency of the model drug and ensuring proper release in in vitro simulated gastrointestinal and colonic conditions. Subsequently, we optimized the release performance for the loaded Cas and Hel type SMCs by coating them either with sodium Alg or Eud. These coating strategies serve a dual purpose: protecting the loaded drug from degradation and preventing premature release, thereby allowing for selective release in the intestines for systemic absorption.

2 | Materials and Methods

2.1 | Materials and Chemicals

5-FU, pepsin from porcine gastric mucosa, porcine bile extract, pancreatin, hemin, vitamin K1, L-cysteine, peptone water, yeast extract, mucin, alginic acid sodium salt, chitosan, acrylic acid, and Tween 80 were purchased from Sigma-Aldrich (St. Louis, MO, USA). Eudragit S-100 was a kind gift of Evonik Corporation (Essen, Germany). Orthophosphoric acid, hydrochloric acid, sodium hydroxide, ethanol, acetone, diethyl ether, dipotassium phosphate, monopotassium phosphate, sodium bicarbonate, magnesium sulfate, and calcium chloride were purchased from Fisher Scientific (Pittsburgh, PA, USA). Potassium chloride, ammonium carbonate, and sodium chloride were purchased from Panreac Applichem (Barcelona, Spain). Magnesium chloride hexahydrate was from Acros Organics (Pittsburgh, PA, USA). While Dulbecco's Modified Eagle Medium (DMEM) was purchased from PAN-Biotech (Aidenbach, Germany), Roswell Park Memorial Institute (RPMI) 1640 medium was purchased from Corning

Inc. (NY, USA). Water was treated in a Milli-Q water purification system (TGI pure system, Houston, TX, USA).

The procedure for collecting, processing, and color-separating bee pollen, as well as confirming the botanical origin and purity of each pollen species, was previously validated through palynological analysis in our earlier studies [11, 24]:

2.2 | Preparation of SMCs and UV Light Treatment

SMCs were isolated from bee pollen using a chemically assisted extraction procedure adapted from an established protocol [11]. Briefly, raw pollen (50 g) was subjected to a series of solvent and aqueous treatments under reflux conditions to remove soluble and structural pollen constituents. The extraction sequence involved successive treatments with acetone (400 mL, 50°C, 3 h), distilled water (400 mL, 50°C, 1 h), acetone (400 mL, 50°C, 3 h), and diethyl ether (400 mL; twice for 2 h and subsequently for 15 h). The remaining solid fraction was then exposed to concentrated phosphoric acid (85%, 400 mL) at 70°C for 8 h. After acid treatment, the microcapsules were recovered by filtration and thoroughly purified through multiple washing steps using water, organic solvents (acetone and ethanol), and acidic (2 M HCl) and alkaline (2 M NaOH) solutions to ensure the complete removal of residual reagents and non-sporopollenin components. The purified SMCs were dried at 45°C for 72 h and stored in a moisture-free environment until further use.

To improve the surface wettability of the extracted microcapsules, UV-C irradiation was applied following the isolation process. The experimental conditions, optimization, and physicochemical characterization associated with the UV treatment are reported in detail in our previous work [25].

2.3 | Loading of Drug Into Natural SMCs

The loading of 5-FU into SMCs was achieved using a vacuum-assisted technique by double loading [26]. Briefly, 100 mg of SMC was mixed in a 1.2 mL solution containing 50 mg of 5-FU, and the suspension was vortexed for 10 min. The sample was placed in a freeze dryer (Telstar Co., Lyoquest 55 Plus, Terrassa, Spain), and a vacuum of 0.5 mbar was applied for 3 h. A second reloading to the SMC, with an additional 50 mg of 5-FU, was performed in the same manner as above. After completing the reloading process, the microcapsules were washed twice with 0.5 mL of water and centrifuged (4500 rpm for 3 min) to remove any 5-FU adhering to the surface. The loaded SMCs were then frozen at −80°C for 30 min and freeze-dried for 24 h, and finally stored in a dry cabinet at room temperature until further use. A placebo sample without 5-FU was prepared using the same method.

2.4 | Formulation of Alg and Eud Coated SMCs

Approximately 100 mg of drug-loaded SMCs were added to 2 mL of 2% aqueous Alg solution and mixed thoroughly [15]. The solution was then transferred dropwise with a 5 mL syringe (20 gauge needle) into approximately 50 mL of 8% calcium chloride solution in a 50 mL beaker over 3 min, with gentle agitation. The mixture was gently stirred for 5 min to harden the Alg gel beads. The Alg beads were collected with filter paper and washed twice with ultra-pure water. The washed beads were placed in a −80°C freezer for 30 min and then freeze-dried for 24 h.

For Eud coating, 100 mg of drug-loaded SMCs were mixed until homogeneously dispersed in 1 mL of 10% Eud dissolved in acetone [21]. The acetone was evaporated at 40°C in a rotavapor (Rotary Evaporator model Hei-VAP from Heidolph, Schwabach, Germany), and the samples were placed in a −80°C freezer for 30 min followed by freeze-drying for 24 h. The dry samples were lightly pulverized with a mortar and stored in a dry environment at room temperature until further studies.

2.5 | Physicochemical Characterization

2.5.1 | SEM

The surface morphology of the samples was examined using a field-emission environmental SEM (FEI Quanta 400 FEG ESEM/EDAX Genesis X4M, FEI Inc., OR, USA). Micrographs were recorded at different magnification levels under an accelerating voltage of 15 kV. Before analysis, the samples were fixed onto conductive carbon adhesive tabs and sputter-coated with a thin Au/Pd layer using an SPI Module Sputter Coater operated at 15 mA for 100 s (SPI Module Sputter Coater, PA, US) to enhance surface conductivity.

2.5.2 | CLSM

Confocal microscopy images were acquired using a Zeiss Axio Imager Z1 microscope coupled with an LSM 510 META confocal system (Carl Zeiss, Baden-Württemberg, Germany), operated with LSM 510 software (version 4.0 SP2). To ensure comparability, all samples were imaged using identical acquisition parameters. Excitation was achieved using argon (488 nm), helium–neon (543 nm), and diode (405 nm) lasers at intensities of approximately 13%, 51%, and 69%, respectively. Pinhole diameters were adjusted to 96 mm (1.02 airy units) for the argon laser, 102 mm (0.98 airy units) for the helium–neon laser, and 112 mm for the diode laser, using a 63× objective lens. Image stacks were collected at scan speeds of 6 or 8 with optical section thicknesses of 1 μm. Three-dimensional deconvolution was performed using AutoQuant X3 software (Media Cybernetics Inc., MD, USA), and the final images were exported as TIFF files and processed using ImageJ software (version 1.47v).

2.5.3 | Laser Diffraction Particle Size Analysis

The particle size distribution of the SMCs was determined by laser diffraction using a Mastersizer 3000 analyzer (Malvern Panalytical Ltd., Malvern, UK) [27]. Measurements were conducted at room temperature with distilled water serving as the dispersing medium. For each sample, five consecutive measurements were performed, and the mean value was reported.

2.5.4 | FTIR Spectroscopy

Chemical characterization of the samples was carried out by FTIR spectroscopy using a Summit X FTIR spectrometer (Thermo Scientific Corp., MA, USA) equipped with an attenuated total reflectance (ATR) accessory featuring a monolithic diamond crystal. Spectra were collected in the range of 4000–600 cm^{-1} at a resolution of 4 cm^{-1}, with each spectrum representing the average of 64 scans. Spectral analysis was performed using OMNIC Paradigm Desktop software (Thermo Scientific Corp., MA, USA).

2.5.5 | TGA

Thermal stability and degradation behavior were evaluated by thermogravimetric analysis using an STA7200RV Thermal Analyzer (Hitachi High-Tech Inc., Tokyo, Japan). Approximately weighed samples were heated from 20°C to 700°C at a constant heating rate of 10°C/min under controlled conditions. The resulting thermograms were analyzed by TA7000 software (Hitachi High-Tech Inc., Tokyo, Japan).

2.6 | Drug Loading Capacity

Drug loading was determined by dispersing approximately 10 mg of the sample in 5 mL of phosphate-buffered saline (PBS, pH = 7.4). The suspension was vortex-mixed for 10 min and subsequently subjected to probe sonication (CY-500, Optic Ivymen System, Barcelona, Spain) at 50% amplitude for 10 cycles of 10 s each at ambient temperature. Following sonication, the mixture was centrifuged at 4500 rpm for 3 min, and the supernatant was collected and filtered through a 0.22 μm syringe membrane. Identical procedures were applied to placebo samples lacking 5-FU to serve as blanks. The absorbance of the filtrates was measured at 266 nm using a UV–Vis spectrophotometer (Zuzi 4255/50, Auxilab, Navarre, Spain). The concentration of 5-FU was calculated using a calibration curve constructed over the range of 1–18 μg/mL ($y = 0.0512x + 0.0152$, $R^2 = 0.999$). Drug loading capacity was calculated according to the equations reported in the literature [21]. Drug loading capacity (%) was defined as the mass of 5-FU encapsulated within the SMCs relative to the total mass of the drug-loaded SMCs (w/w%).

$$Amount\ of\ drug\ (mg) = (Absorbance \times dilution\ factor) / (Slope \times 1000)$$

$$Loading\ (\%) = (Amount\ of drug\ released / Weight\ of drug\ loaded\ SMCs) \times 100$$

Additionally, the theoretical drug loading capacity for both Cas and Hel type SMCs was calculated based on the initial mass ratio of drug to carrier used during the loading process [21]. Given the total batch composition (200 mg), the theoretical loading was estimated to be 50% for both SMCs types.

2.7 | In Vitro Drug Release Under Simulated Gastrointestinal and Colonic Conditions

The release profile of 5-FU from the microcapsule formulations was investigated under conditions designed to reproduce the physicochemical transitions encountered during gastrointestinal transit. The study consisted of successive incubation in simulated gastric fluid (SGF, pH = 2.0), simulated intestinal fluid (SIF, pH = 7.0), and simulated colonic fluid (SCF, pH = 7.4) environments, following previously reported protocols [28, 29]. Dialysis membranes were selected for this study due to their semi-permeable nature, which allows the released drug to diffuse into the surrounding medium while retaining the microcarrier system, thereby enabling reliable assessment of release kinetics under sink conditions and demonstrating good correlation with in vivo behavior [30]. For this purpose, 10 mg of each sample was sealed within dialysis tubing (MWCO: 14 kDa) containing 5 mL of SGF. The bags were immersed in 50 mL of the same medium and maintained at 37°C with continuous shaking at 100 rpm for 2 h. The incubation medium was then replaced sequentially with SIF for 3 h and SCF for up to 24 h. At defined time points, aliquots (2 mL) were collected from the release medium and immediately replenished with fresh fluid to preserve sink conditions. Release studies were conducted under sink conditions, as the solubility of 5-FU (~12 mg/mL) in the release media was significantly higher than the maximum drug concentration present during the experiments, ensuring that dissolution was not solubility-limited. The withdrawn samples were filtered (0.22 μm) and analyzed spectrophotometrically at 266 nm using placebo-treated media as blanks. Detailed formulations of the simulated digestive and colonic media, including enzyme composition and fecal sample preparation, have been described in the Supporting Information and elsewhere [28]. The amount and cumulative percentage of released 5-FU were determined using the following equations [20]:

$$Concentration\ of\ drug\ (mg/mL) = (Absorbance - intercept) / \text{slope}$$

$$Amount\ of\ 5-FU\ (mg) = (Concentration \times Dissolution\ bath\ volume)$$

$$Cumulative\ release\ (\%) = (Volume\ of\ withdrawn\ (mL) / Bath\ volume\ (mL)) \times P(t-1) + Pt$$

where P_t is the rate of free release at time t, and $P_{(t-1)}$ is the rate of free release before t.

Cumulative release (%) was calculated based on the total amount of drug loaded into the SMCs and represents the fraction of encapsulated drug released over time; this calculation accounts for the amount of drug removed during each sampling step, with replacement by fresh medium, to ensure accurate determination of the total released drug.

2.8 | 5-FU Release Kinetics Studies

Understanding the release behavior of an active compound is essential for evaluating the performance of drug delivery systems, particularly those designed for controlled or site-specific administration. In this study, the release profiles of 5-FU from SMCs were quantitatively assessed using established kinetic approaches to elucidate the underlying release mechanisms and compare formulation performance. Model fitting was carried out using commonly employed mathematical descriptions of drug release behavior, and the goodness of fit was evaluated based on correlation coefficients (R^2), release rate constants (k), and, where applicable, release exponents

(n). These analyses were used to support interpretation of diffusion- and matrix-controlled release characteristics relevant to microcarrier-based delivery systems. The theoretical background, governing equations, plotting methods, and interpretation criteria for the zero-order, first-order, Higuchi, and Korsmeyer–Peppas kinetic models are provided in the Supporting Information [31].

2.9 | Mucoadhesive Evaluation of SMCs

TA.XTplus Texture Analyzer (Stable Micro System, Godalming, UK) was used to measure the bioadhesion bond strength of SMCs, SMCs coated with Alg and Eud, and also control materials, namely chitosan and acrylic acid [14, 32]. For the analysis, 150 mg of the sample was used to produce a disc (diameter = 1.3 cm) by applying a compression force of 10 tons for 20 s using a manual press. The disc was fixed to the vertically moving probe (20 mm) with double-sided tape. A constant temperature (37°C) water bath is placed on the lower part of the texture analyzer. An agar plate (diameter = 9.5 cm) with a 2 mL of mucin (5% mucin, 95% water, pH = 7.0) layer was placed in the water bath. The analytical probe holding the samples was moved down to the mucin surface at a constant speed of 0.1 mm/s, and a contact force of 0.5 N was applied. At the end of the contact time set to 60 s, the probe was moved 5 mm from the surface in the upward direction with a constant speed of 0.1 mm/s. The force required to detach the disc from the mucin surface was determined from the resulting force-time plot, and then it was converted into a force-distance plot. The two important data generated in the mucoadhesive test mode were used to evaluate the bioadhesive properties of the samples: (i) the mucoadhesive force corresponding to the separation maximum force (N), and the work of mucoadhesion calculated from the area under the curve (AUC) from the force-distance plot. Detachment-force values depend strongly on test conditions (probe size, preload, contact time, mucus source). We therefore report both peak force and calculated work of adhesion, noting that work tends to be less sensitive to experimental variables. The work of mucoadhesion (mJ/cm^2) was calculated using the following equation [32]:

$$Work\ of\ mucoadhesion\ \left(mJ/cm^2\right) = \frac{AUC}{\pi r^2}$$

where πr^2 is the mucosal surface area in contact with the disc.

2.10 | Biocompatibility Analysis of SMCs

The biocompatibility of Cas and Hel derived SMCs was evaluated using the sulforhodamine B (SRB) assay on Vero cells, a non-tumor kidney epithelial cell line [33]. The cell line was sourced from the European Collection of Authenticated Cell Cultures. Cells were maintained in DMEM supplemented with RPMI 1640 medium containing 10% fetal bovine serum, 2 mM glutamine, 100 U/mL penicillin, and 100 μg/mL streptomycin, and cultured at 37°C in a humidified atmosphere containing 5% CO_2.

For the assay, adherent cells were detached using trypsin and seeded into 48-well plates at a density of 1.0×10^4 cells per well. After a 24 h incubation period to allow cell attachment, the cultures were exposed to SMC suspensions prepared in water at concentrations ranging from 0.125 to 8 mg/mL. Following 48 h of treatment, cell growth was quantified using the SRB assay. Dose–response curves were plotted, and the growth inhibition, defined as the concentration required to inhibit 50% of cell proliferation, was calculated as the 50% growth inhibition (GI_{50}) values relative to untreated control cells and expressed in μg/mL. All samples were analyzed in two independent experiments, each performed in duplicate. Ellipticine (0.38–12.3 μg/mL) was used as a positive.

2.11 | Statistical Analysis

Statistical analysis was performed using GraphPad Prism 9.5.1 (San Diego, CA, USA). A two-tailed t-test and one-way ANOVA followed by Tukey's post hoc test were applied to evaluate the statistical significance of differences between drug release profiles and other quantitative parameters across different formulations. The two-tailed t-test was used to compare the means between two independent groups (e.g., Cas vs. Hel SMCs) to determine whether a significant difference existed in their behavior. Meanwhile, ANOVA with Tukey's post hoc test was employed when comparing more than two groups (e.g., uncoated, Alg-coated, and Eud-coated SMCs), allowing for the identification of specific pairs of groups that differed significantly. All experiments were conducted with at least three independent replicates, and the data are presented as mean ± SD. Significance levels of the p-value are denoted as follows: 0.01 to 0.05 (*), 0.001 to 0.01 (**), and < 0.001 (***).

3 | Results and Discussion

3.1 | Preparation and Morphological Characterization of SMCs and Drug Loading

To evaluate the potential of SMCs derived from Cas and Hel bee pollen as drug delivery carriers, their structural integrity, morphology, and particle size characteristics were analyzed using SEM, CLSM, and laser diffraction techniques. Efficient compound loading into SMCs requires the complete removal of internal cytoplasmic material while preserving the exine shell and aperture structures [19]. SEM analysis confirmed that the three-step chemical treatment successfully removed internal contents and the external oily coat, exposing clean and intact sporopollenin shells, Figure 1a. Cas type SMCs exhibited a flattened, rugulate morphology, typical of Cas pollen grains, while Hel type SMCs retained a more spherical form with perforate-striate ornamentation. Notably, both SMC types displayed a well-defined tricolporate aperture, a crucial feature for compound entry and exit. The preservation of these apertures highlights the suitability of both pollen types for subsequent loading and release of therapeutic agents. Further insights into the internal cavity of the SMCs were obtained using CLSM. Natural pollen grains exhibited strong intrinsic autofluorescence from blue to red channels, particularly localized in the cytoplasmic regions and cell wall, consistent with the presence of proteins, lipids, and phenolic compounds, Figure 1b [15]. In contrast, SMCs displayed minimal to no autofluorescence in the inner cavity, strongly

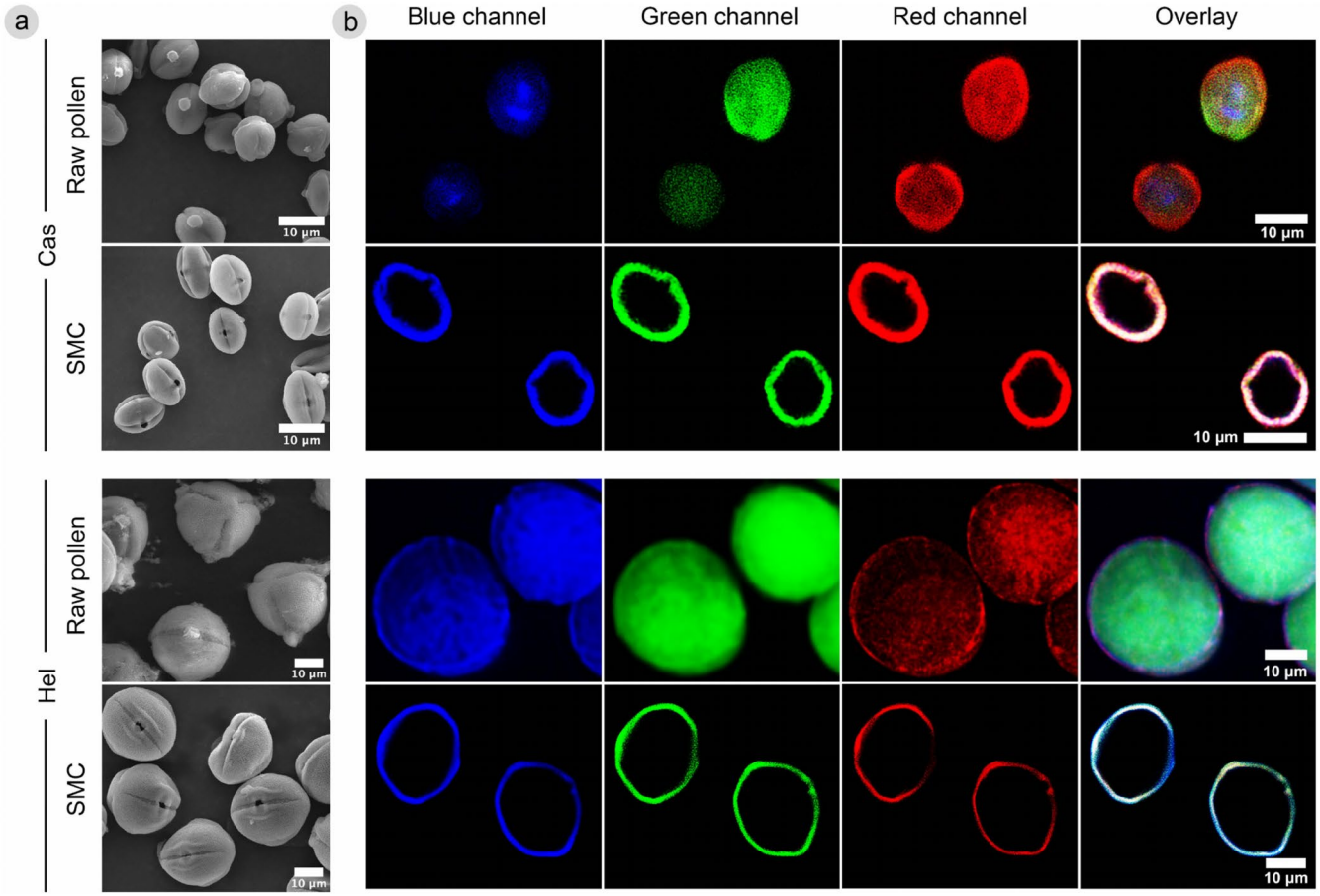

FIGURE 1 | Microscopic characterization of Cas and Hel type bee pollen before and after SMCs purification. (a) SEM images showing the surface morphology of raw pollen grains and the corresponding SMCs after chemical treatment. (b) CLSM images highlighting the removal of internal contents from pollen grains in SMCs, based on the loss of autofluorescence in the inner cavity.

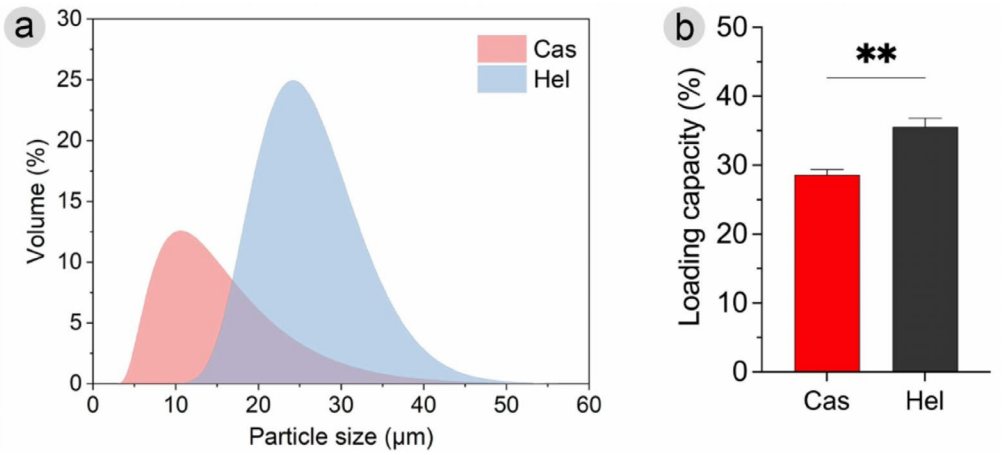

FIGURE 2 | (a) Particle size distribution of Cas and Hel type SMCs measured using laser diffraction, presented as spherical diameters (mean ± SD, $n = 5$). (b) Drug loading capacities (%) of 5-FU into Cas and Hel SMCs using the vacuum loading method (mean ± SD, $n = 3$). Statistical significance was evaluated using a two-tailed t-test. $^{**}p < 0.01$.

suggesting the effective removal of pollen internal macromolecules. This observation confirms that the purification process cleared the internal space, making it available for efficient drug encapsulation.

Another critical parameter for drug delivery is particle size, which directly influences surface area, diffusion characteristics, and release behavior. Laser diffraction analysis revealed that Hel derived SMCs had a significantly larger average diameter (24.1 ± 0.1 μm) compared with Cas derived SMCs (11.2 ± 0.1 μm), as shown in Figure 2a. The low standard deviations reflect the high repeatability of the laser diffraction measurements under controlled dispersion conditions. Morphological observations on both types of SMCs show that they maintain their structural

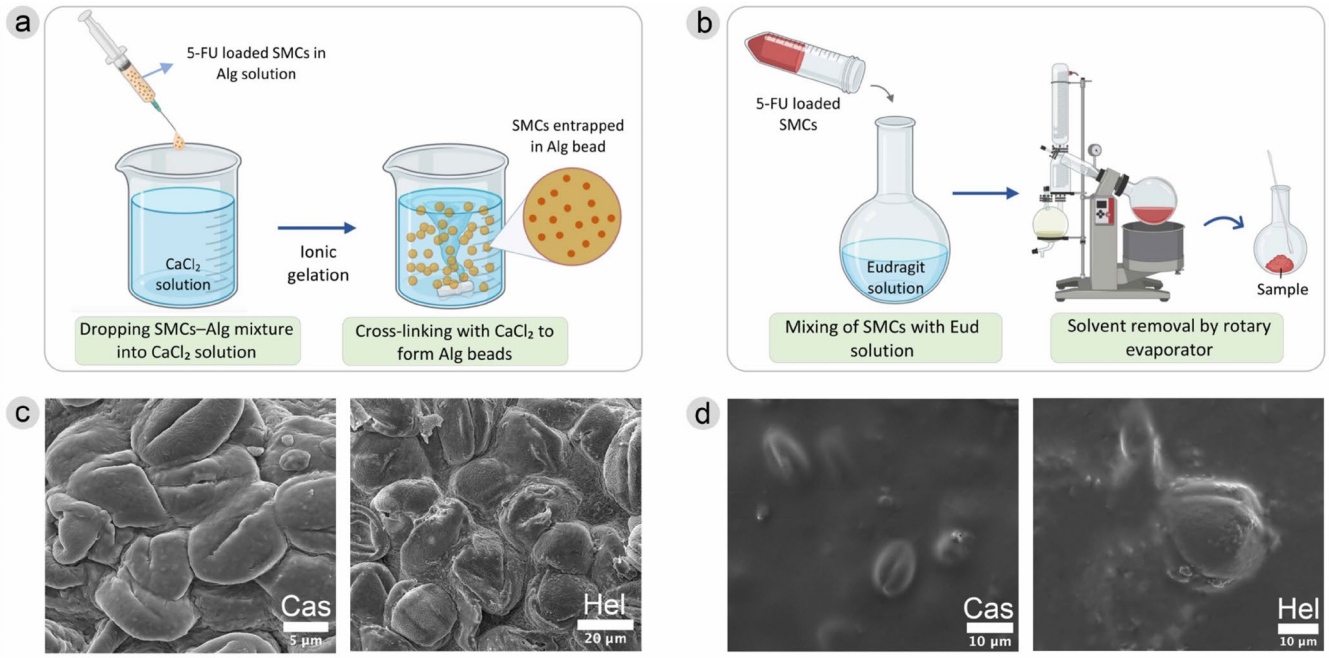

FIGURE 3 | Schematic representation of the preparation of 5-FU-loaded SMCs incorporated into (a) Alg beads and (b) coated with Eud. SEM images of 5-FU-loaded Cas and Hel type SMCs coated with (c) Alg and (d) Eud polymers.

integrity without any denaturation and exhibit size uniformity. We have also previously reported details regarding parameters such as porosity, surface topography, pore count, and pore size for the types of SMCs studied in this work [11, 20, 24]. This is important as any proposed drug delivery system for controlled and site-specific delivery requires uniformity in size and shape for efficacy and performance, and controlling product quality in encapsulation processes can be a major challenge [34]. It is also important to highlight that these pollen types were selected for their distinct morphological and dimensional characteristics, which are expected to influence loading efficiency and drug release profiles.

Following the morphological characterization of the SMCs, the model anticancer drug 5-FU was encapsulated using a vacuum-assisted loading technique. The resulting loading capacities were 28.6% ± 0.8% for Cas type SMCs and 35.5% ± 1.3% for Hel type SMCs, with Hel type SMCs exhibiting a statistically significant ($p < 0.05$) higher loading efficiency, Figure 2b. The rationale for employing a two-step loading procedure lies in the dual role of the natural apertures in the pollen wall. While these openings facilitate the diffusion of drug molecules into the inner cavity, they also enable premature leakage during preparation and washing steps, potentially reducing loading efficiency [20]. Repeating the vacuum loading process mitigated this effect and increased drug entrapment. The loading efficiencies achieved in this study surpass previously reported values for 5-FU (16.3%) [21] and aspirin (26.7%) [17] loaded into *Lycopodium clavatum* SMCs, as well as metformin (15.2%) [7] encapsulated in *Phoenix dactylifera* L. SMCs. This suggests that the choice of pollen type and the optimization of the loading process have a substantial impact on drug encapsulation efficiency. A notable trend was the loading performance of Hel type SMCs. This can be attributed to several interrelated factors. Larger microcapsules typically possess greater internal volumes and higher porosity, providing more space and channels for the drug to diffuse and be retained [4, 35]. Additionally, their lower surface curvature can reduce resistance to molecular penetration, while enhanced structural stability during vacuum cycles helps prevent loss of loaded material [20]. These characteristics contribute to the higher drug loading efficiency observed in Hel type SMCs compared with smaller Cas type SMCs.

As mentioned in section 2.6, the theoretical maximum loading capacity of 5-FU in both Cas and Hel type SMCs was estimated to be ~50%; however, the experimentally obtained values (28.6% for Cas and 35.5% for Hel) were lower, indicating incomplete utilization of the SMCs' cavity volume. This difference can be attributed to limited accessibility of internal cavities, diffusion constraints, and partial drug loss during loading and washing, as well as leakage through natural apertures. Based on the vacuum-assisted loading mechanism, the drug is expected to be primarily distributed within the SMCs' cavity and adsorbed onto internal surfaces, with a smaller fraction near aperture regions.

Our findings indicate that the loading capacity of bee pollen SMCs is comparable to other SMC systems developed for gastrointestinal delivery [7, 15, 16, 18, 19, 21, 26]. However, as observed in these previous systems, including our work [20], SMCs alone do not provide sufficient resistance to sustain drug release over extended periods. To address this limitation and achieve a sustained, tunable release profile, we incorporated 5-FU loaded Cas and Hel type SMCs either into Alg (2% w/v) beads or Eud coating (10% w/v). Figure 3a shows that loaded SMCs were produced within an Alg solution through ionic cross-linking with calcium chloride, resulting in a gel-like structure that entrapped the SMCs within Alg beads. Figure 3b, in contrast, illustrates that loaded SMCs were coated with Eud using a solvent evaporation method. SEM analysis was performed to further examine the fabricated Alg beads and Eud coatings. The SEM images

confirmed that the Cas and Hel types of drug loaded SMCs were successfully coated with Alg, Figure 3c, and Eud polymer, Figure 3d. In addition to SEM analysis, FTIR spectroscopy was used to analyze and confirm chemical interactions between the SMCs, drug, and coating materials, while TGA was employed to verify successful drug loading and coating, as well as to assess the thermal behavior of the SMCs and formulations.

3.2 | Chemical Characterization and Thermal Stability

FTIR spectroscopy revealed the characteristic peaks corresponding to 5-FU, Alg, and Eud, confirming the successful loading and coating processes, Figure 4. The FTIR spectrum of 5-FU, Figure 4a, displayed identifiable bands near 3070 cm^{-1}, 1720 cm^{-1}, 1650 cm^{-1}, 1426 cm^{-1}, and 1242 cm^{-1}, which are attributed to N—H stretching, C═O stretching, C═C/C═O stretching, C—N and C—F vibrations, respectively [20, 36]. Alg exhibited its typical bands at 3320 cm^{-1} (OH stretching), 1594 cm^{-1} (asymmetric COO^- stretching), 1405 cm^{-1} (symmetric COO^- stretching), and 1024 cm^{-1} (C—O stretching) [7, 37]. Eud showed a broad OH stretching band between 3540 and 3250 cm^{-1}, along with characteristic bands at 1724 cm^{-1} (strong C═O stretching), 1436 cm^{-1} (asymmetric CH_3 bending), 1246 cm^{-1} (C—O—C asymmetric stretching), and 1146 cm^{-1} (C—O stretching), Figure 4a [16, 38, 39].

The FTIR spectra of Cas and Hel type SMCs also showed chemical similarities, including a broad OH stretching band at 3370 cm^{-1} [40], which remained visible after drug loading, Figure 4b,c. The N—H stretching band of 5-FU overlapped with the broad OH band, suggesting interactions between the drug and the hydroxyl groups of sporopollenin. The peak at 1680 cm^{-1} in unloaded SMCs, attributed to asymmetric C═C stretching from aromatic and phenolic compounds within sporopollenin [41], shifted to 1670 cm^{-1} and became more intense after 5-FU loading, indicating successful encapsulation and possible hydrogen bonding interactions. Upon polymer coating, this feature becomes a shoulder due to the stronger bands at 1603 cm^{-1} with Alg and 1720 cm^{-1} with Eud, reflecting changes in the chemical environment. In addition, the band at 1432 cm^{-1} in Cas type SMCs, assigned to asymmetric stretching of carboxylate anions (COO^-) [40, 41], became more intense after 5-FU encapsulation. In Hel type SMCs, the corresponding peak initially at 1418 cm^{-1} shifted to 1432 cm^{-1} post-loading, showing similar enhancement. These peaks further shifted slightly to 1420 cm^{-1} (Alg-coated) and 1434 cm^{-1} (Eud-coated), suggesting successful polymer interaction. Likewise, the weak C—O stretching peak at 1244 cm^{-1} in SMCs shifted to 1234 cm^{-1} after drug loading and subsequently shifted to 1250 cm^{-1} and 1244 cm^{-1} following Alg and Eud coating, respectively [11, 20, 40].

Collectively, these spectral changes provide strong evidence of effective 5-FU encapsulation within the SMCs and the subsequent interaction with Alg and Eud coatings. The observed shifts in functional group vibrations support the formation of chemical interactions between the components. These findings align well with previously reported FTIR analyses of 5-FU-loaded *Phoenix dactylifera* SMCs [16], metformin-loaded *Lycopodium clavatum* and *Phoenix dactylifera* SMCs [7], and their respective polymer-coated derivatives. Moreover, the similarities in spectral patterns of formulations further validate the reproducibility and reliability of our encapsulation and coating approach.

TGA was employed to investigate the thermal properties of the various materials, SMCs, and formulations used in this study. Specifically, we aimed to determine whether SMCs influenced the thermal stability of the drug and to confirm successful drug incorporation. Figure 5 shows the TGA profiles of the studied materials, SMCs, and formulations up to 700°C.

The thermal degradation of pure 5-FU occurred in two distinct stages: (i) the first decomposition step took place between ~50°C and 203°C, likely due to the evaporation of adsorbed water; (ii) the second stage, occurring between ~230°C and 308°C and responsible for 98.2% weight loss, was attributed to structural decomposition of 5-FU, particularly the cleavage of the pyrimidine ring, Figure 5a [42, 43]. For Alg, three main degradation stages were identified: (i) the loss of physically adsorbed and bound moisture at ~50°C–160°C (12.2% weight loss), (ii) cleavage of glycosidic bonds in the Alg backbone at ~200°C–265°C (41% weight loss), and (iii) degradation of uronic acid units between ~270°C and 480°C (10% weight loss) [7, 44]. In the case of Eud, the initial degradation up to ~170°C was due to water evaporation, while the scission of side chains occurred between ~200°C and 250°C. The most significant degradation took place between ~250°C and 450°C (90% weight loss), corresponding to the breakdown of ester bonds and the methacrylic polymer backbone [45].

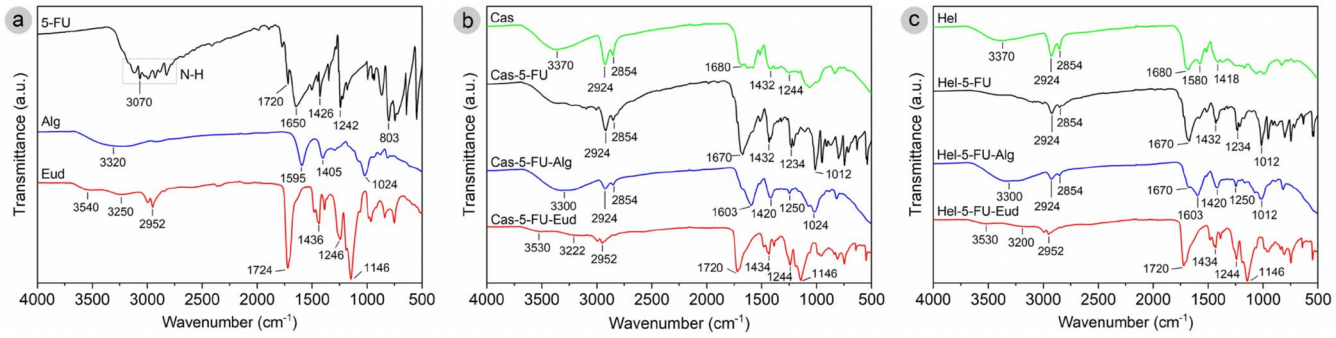

FIGURE 4 | FTIR spectral analysis of 5-FU, polymers, and SMC formulations. (a) FTIR spectra of pure 5-FU and the Alg and Eud polymers. (b) FTIR spectra of Cas type SMCs before and after 5-FU loading and polymer coating. (c) FTIR spectra of Hel type SMCs before and after 5-FU loading and polymer coating.

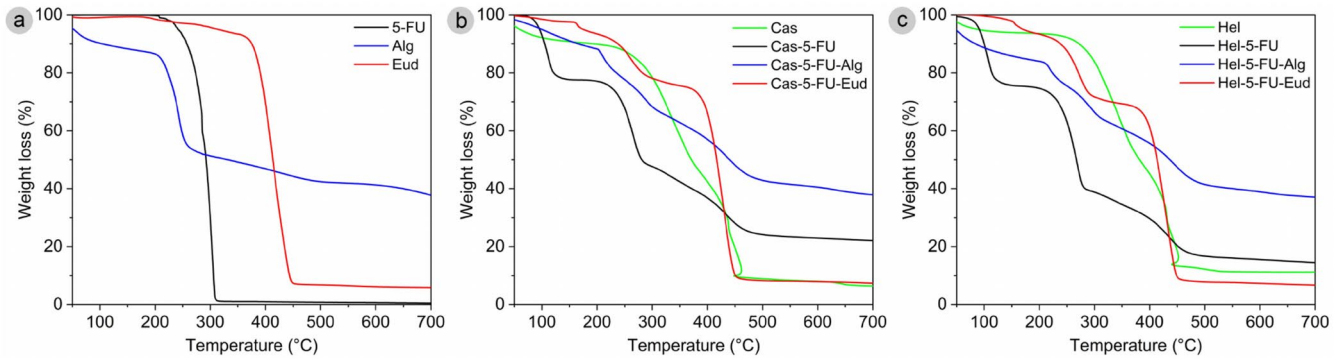

FIGURE 5 | Thermal stability profiles of 5-FU, polymers, and SMC formulations evaluated by TGA. (a) TGA thermograms of pure 5-FU, Alg, and Eud. (b) TGA thermograms of Cas type SMCs, including unloaded, 5-FU loaded, and polymer-coated variants. (c) TGA thermograms of Hel type SMCs in the same formulation states as in (b).

The thermal degradation behaviors of Cas and Hel type SMCs were comparable and occurred in three main stages, Figure 5b,c: (i) evaporation of weakly bound water at ~50°C–160°C (7%–9% weight loss), (ii) degradation of residual components such as hemicellulose, cellulose, or pectin at ~200°C–400°C (47%–49% weight loss), and (iii) partial decomposition of the sporopollenin wall at ~400°C–500°C (34%–36% weight loss) [11, 24, 41], which lacks cellular content. In addition, the maximum degradation temperatures for Cas and Hel type SMCs were approximately 453°C and 451°C, respectively. These values are in line with those reported for SMCs purified from *Lycopodium clavatum* pollen (~441°C, 92.5% weight loss) [17] and *Corylus avellana* pollen (~471°C) [46], supporting the reliability of our findings.

Drug-loaded SMCs and their polymer-coated derivatives displayed additional degradation steps. Compared with the empty SMCs, the 5-FU-loaded Cas and Hel types exhibited a new degradation peak and a slight increase in their maximum degradation temperatures, providing strong evidence for successful drug encapsulation. However, drug loading did not significantly alter the thermal stability of the 5-FU itself, as its degradation temperature remained close to ~310°C. Further inspection of the TGA thermograms reveals subtle but consistent shifts in the maximum degradation temperature upon drug loading and coating. For Cas SMCs, it increased from 453°C (empty) to 458°C (5-FU loaded); for Hel SMCs, from 451°C to 460°C. These upward shifts suggest that encapsulated 5-FU interacts with the sporopollenin polymer (e.g., via hydrogen bonding or π-π interactions), conferring moderate thermal stabilization. Coating with Alg or Eud further raised degradation temperature to 465°C–471°C, reflecting the additional thermal barrier provided by the polymer layers, albeit not to a significant degree. While these changes are modest, they qualitatively support successful encapsulation and coating, complementing the quantitative loading data obtained by spectrophotometry. Another interesting point was the partial decrease in the prominence of thermal degradation peaks in drug-loaded SMCs coated with Alg. This was most likely due to the overlapping degradation temperatures of the drug, the SMCs, and the polymers. It is important to note that the degradation behavior of multi-component formulations, including SMCs, pure drugs, and polymers, may differ from that of the individual components due to possible chemical interactions. Similar findings have been reported in the literature. For example, Uddin et al. [47] observed that the presence of cellulose and other residual materials altered the thermal degradation profile of sporopollenin. Another study reported that the thermal stability of *Corylus avellana* derived SMCs increased upon loading with pantoprazole, possibly due to the formation of hydrophobic interactions or other stabilizing molecular interactions between the drug and sporopollenin [46].

3.3 | Drug Release Behavior in the Gastrointestinal and Colonic Environment

After confirmation that natural SMCs produced from bee pollen pellets are highly promising carriers for the encapsulation of the anticancer drug 5-FU, we evaluated the in vitro release profiles of 5-FU from these SMCs, differing in morphology and further modified via Alg or Eud coating, under continuous simulated gastrointestinal and colon conditions: SGF (pH = 2.0), SIF (pH = 7.0), and SCF (pH = 7.4).

As shown in Figure 6a,b, uncoated Cas and Hel type SMCs released 78% ± 4% and 68% ± 3% of 5-FU, respectively, at the end of 2 h in SGF. After 3 h in SIF, cumulative drug release reached 83% ± 3% for Cas type and 74% ± 5% for Hel type SMCs. Prolonged exposure in SCF up to 24 h resulted in total drug release values of 87% ± 5% for Cas SMCs and 78% ± 3% for Hel SMCs. Both types of SMCs exhibited a biphasic release profile, characterized by an initial burst release during the first h, followed by a plateau release phase extending up to 24 h.

Although the release behaviors in gastrointestinal and colonic media were broadly similar, Cas type SMCs consistently exhibited higher release rates than Hel type SMCs. This difference may be attributed to the larger size of Hel type SMCs, which increases the diffusion distance between the encapsulated drug and the external surface, thereby slowing release [48]. Additionally, the reduced interfacial area between SMCs and the release medium could have contributed to the slower release profile of drug molecules from larger SMCs [22]. These findings align with the previous report on SMCs derived from various pollen types, indicating that such structures do not significantly hinder drug release across sequential media [20]. The relatively rapid release observed here may be further explained

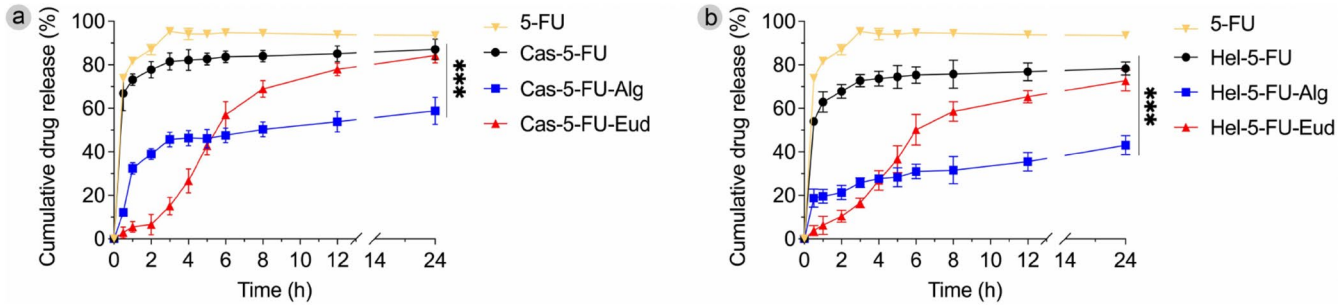

FIGURE 6 | Cumulative release profiles of 5-FU from SMC formulations under simulated gastrointestinal and colonic conditions. (a) Cas type SMCs and their Alg and Eud coated derivatives. (b) Hel type SMCs and their Alg and Eud coated derivatives. Drug release is presented as mean ± SD ($n = 3$). ***$p < 0.001$.

by the structural characteristics of the SMCs, specifically, the presence of three large apertures on each microcapsule, which likely facilitated diffusion. Although direct spatial mapping was not performed, indirect evidence, including the effectiveness of repeated vacuum loading, removal of surface-associated drug during washing, high release from uncoated SMCs (78%–87% within 24 h), and SEM images supports predominant internal encapsulation rather than surface adsorption. This heterogeneous distribution likely contributes to the initial burst release followed by sustained release behavior. Nevertheless, further studies using advanced imaging techniques (e.g., fluorescent labeling) would provide more definitive confirmation of drug localization/distribution.

To enhance protection of the drug in acidic environments and to achieve sustained, tunable release in intestinal regions, we modified the loaded SMCs by incorporating them into Alg beads or coating them with Eud. Alg and Eud concentrations were selected based on prior studies optimizing formulations for controlled release of compounds from SMCs [7, 15, 16, 21]. When 5-FU-loaded Cas type SMCs were incorporated in Alg beads, a lower burst effect was observed within the first h, with controlled release over 24 h, Figure 6a. Cas type SMCs in Alg beads showed cumulative drug release values of 39% ± 2%, 46% ± 4%, and 59% ± 6% in SGF, SIF, and SCF, respectively. Corresponding values for Hel type SMCs were lower: 21% ± 3%, 28% ± 4%, and 43% ± 4%, respectively. The differences in drug release between Cas and Hel type SMCs in Alg beads were statistically significant in all media ($p < 0.05$). These results confirm that SMCs embedded in Alg beads, prepared via ionic gelation, effectively reduced initial burst release and enabled sustained gastrointestinal and colon-specific drug delivery. Release profiles were also found to vary according to SMC morphology. For Eud coated microcapsules, drug release from Cas type SMCs was 6% ± 5% in SGF and 43% ± 4% in SIF, while Hel type SMCs released 10% ± 3% and 37% ± 6% under the same conditions. After 24 h, cumulative release reached 84% ± 4% for Cas and 73% ± 5% for Hel type SMCs. No significant differences were observed between the two types of Eud coated SMCs in SGF and SIF, but their cumulative release values at 24 h differed significantly ($p < 0.05$). Additionally, it should be noted that complete recovery of the initially loaded drug may not be achieved due to factors such as adsorption to the dialysis membrane or minor degradation. Therefore, cumulative release values represent the fraction of drug released into the medium under the experimental conditions. Eud S-100 is known for its pH-dependent solubility, insoluble in acidic conditions and increasingly soluble at pH = 7.0 and above, which supports the observed release behavior, facilitating delayed and controlled release in the colon [49]. After 24 h, the amount of drug remaining in Alg coated Cas and Hel type SMCs was 20%–30% higher than in Eud coated ones. These results are consistent with previous findings by Raish et al. [16], who reported that drug-loaded SMCs derived from *Phoenix dactylifera* pollen and coated with Eud exhibited slower, more controlled release profiles, with reductions of 8% in SGF and 12% in SIF compared with uncoated SMCs.

While natural SMCs alone exhibit limited ability to achieve site-specific and controlled drug release, these limitations can be effectively overcome through Alg or Eud coating, which serve as diffusion barriers and tuning agents. These modified systems present strong potential for site-specific drug delivery in treating diseases affecting the gastrointestinal tract or colon [50].

3.4 | Drug Release Kinetic Modeling

To better understand the mechanisms underlying 5-FU release from SMCs, the experimental data were fitted to four common kinetic models: zero-order, first-order, Higuchi, and Korsmeyer–Peppas. The correlation coefficients (R^2), rate constants (k), and release exponent (n) values are presented in Table 1. Among the uncoated samples, both Cas and Hel type SMCs exhibited the highest R^2 values for the Korsmeyer–Peppas model (0.938 and 0.937, respectively), followed by the Higuchi model (0.857 and 0.860). This indicates that drug release from uncoated SMCs was predominantly governed by diffusion through the sporopollenin biopolymer [17], consistent with the porous nature of SMCs and the presence of natural apertures facilitating drug escape. The release exponent n values for both Cas (0.068) and Hel (0.093) types were well below 0.45, suggesting a Fickian diffusion mechanism [17].

Upon Alg coating, the release kinetics remained diffusion-dominated, with the Higuchi model yielding the best fit ($R^2 = 0.869$ for Cas-Alg and 0.955 for Hel-Alg). The Korsmeyer–Peppas model also showed high correlation ($R^2 = 0.925$ and 0.962), with slightly increased n values (0.205 for Cas-Alg and 0.252 for Hel-Alg), indicating a shift toward anomalous (non-Fickian) transport. This suggests that, while diffusion was still the primary mechanism, polymer swelling and matrix relaxation may have contributed to drug release. These findings align

TABLE 1 | Kinetic parameters and model fit analysis of drug release from Cas and Hel type SMCs and their derivatives coated with Alg and Eud polymer.

	Zero-order kinetics		First-order kinetics		Higuchi model		Korsmeyer-Peppas model		
Sample	R^2	k_0	R^2	k_1	R^2	k_H	R^2	k_{KP}	n
Cas	0.744	1.397	0.791	0.030	0.857	5.783	0.938	74.087	0.068
Cas-Alg	0.772	2.228	0.800	0.017	0.869	9.120	0.925	33.735	0.205
Cas-Eud	0.965	9.212	0.951	0.075	0.922	38.516	0.935	3.919	1.390
Hel	0.748	1.696	0.784	0.025	0.860	7.015	0.937	63.840	0.093
Hel-Alg	0.903	1.804	0.913	0.011	0.955	7.156	0.962	19.092	0.252
Hel-Eud	0.975	8.197	0.966	0.055	0.944	31.121	0.977	5.386	1.162

Note: R^2: correlation coefficient, k: release rate constant, n: release exponent.

with the experimental release data, where Alg beads significantly reduced the initial burst and extended the release period. In contrast, Eud coated SMCs showed distinct kinetic behavior. For both Cas-Eud and Hel-Eud formulations, the best fit was achieved with the Korsmeyer–Peppas model, showing the highest R^2 values (0.935 and 0.977, respectively). Notably, the n values for Cas-Eud (1.390) and Hel-Eud (1.162) were greater than 1, indicating super case II transport [31]. This type of release is typically associated with polymer erosion and relaxation-controlled mechanisms [51], which is consistent with the pH-dependent solubility and swelling behavior of Eud in intestinal and colonic environments. The excellent fit to the zero-order model ($R^2 = 0.965$ for Cas-Eud, 0.975 for Hel-Eud) also suggests that the drug was released at a near-constant rate, supporting the hypothesis of controlled erosion as the dominant mechanism [31]. The kinetic models applied in this study are consistent with those previously reported for SMCs derived from species such as *Echium* sp., *Jasione* sp., *Papaver* sp., *Amaranthaceae*, and *Cistus* sp. [20], and also align with model compatibilities observed in studies evaluating release kinetics and mechanisms in various polymer-based microcapsules and natural SMC systems [17, 46, 52]. Although R^2, k, and n values provide a useful comparison among release models and are commonly used in the drug delivery literature [7, 17, 46], the final interpretation was made cautiously, and the selected model is presented as the one that best describes the data under the tested conditions. It should be noted that model selection was based primarily on these parameters, as residual analysis or formal model comparison would provide more rigorous discrimination; however, with limited time points, such tests would have limited statistical power. Therefore, the kinetic parameters should be taken as supportive descriptions of the release behavior rather than definitive proof of the mechanism.

The kinetic modeling results reinforce the observations from the release experiments. Uncoated SMCs primarily followed Fickian diffusion due to their porous structure and large apertures. Alg coated SMCs exhibited a more complex release profile, involving a combination of diffusion and polymer relaxation. Eud coated formulations provided the most controlled and extended release, governed by polymer erosion and swelling in response to pH. These findings confirm that polymeric coatings not only reduce the burst effect and prolong release but also fundamentally alter the release mechanism. Such tunability is critical in the design of site-specific drug delivery systems for gastrointestinal and colonic applications.

3.5 | Bioadhesive Properties of SMCs

In vitro assays were conducted to evaluate the bioadhesive properties of SMCs and to compare them with commonly used polymers in drug delivery systems. Detachment force and work of adhesion were measured via tensile testing, which simulates in vivo-like conditions and provides insight into the relative mucoadhesiveness of the materials [23]. These parameters are widely accepted as preliminary indicators of a material's ability to adhere to mucus or biological tissues [53].

As shown in Figure 7, uncoated SMCs exhibited better mucin adhesion compared with both their coated counterparts and reference polymers such as chitosan and acrylic acid. For Cas type SMCs, the maximum detachment force reached 1.13 N, whereas Alg and Eud-coated variants showed lower values of 0.76 N and 0.77 N, respectively, with no significant ($p < 0.05$) difference between the two coatings, Figure 7a. Hel type SMCs demonstrated even higher adhesion, with a peak detachment force of 2.15 N, Figure 7b. Overall, Hel type SMCs and their coated versions showed greater force resistance than the Cas type SMCs and their coated counterparts, indicating stronger mucoadhesive potential. The Hel type SMCs present a highly corrugated, spiked exine that increases contact area. According to mechanical adhesion theory, surface roughness and protrusions (echini) promote stronger binding by interlocking with the mucus network. In addition, sporopollenin's surface chemistry (hydroxyl, carbonyl, and carboxyl) can form multivalent hydrogen bonds and electrostatic interactions with mucin [25]. In a similar study, Diego-Taboada et al. [14] measured the mucin adhesion of *Lycopodium clavatum* SMCs, reporting detachment forces near 300 mN for powdered SMCs and 600 mN for tableted formulations after 4 min of contact, highlighting comparable trends in mucoadhesiveness. In a study conducted by Baloglu, it was reported that the detachment force of mucin discs for poly(acrylic acid) and poly(acrylic acid)–cysteine polymers can range between 3.3 N and 3.4 N [54], while another study testing the efficacy of oromucosal drug delivery systems developed using lipid-based microparticle formulations, the patches exhibited

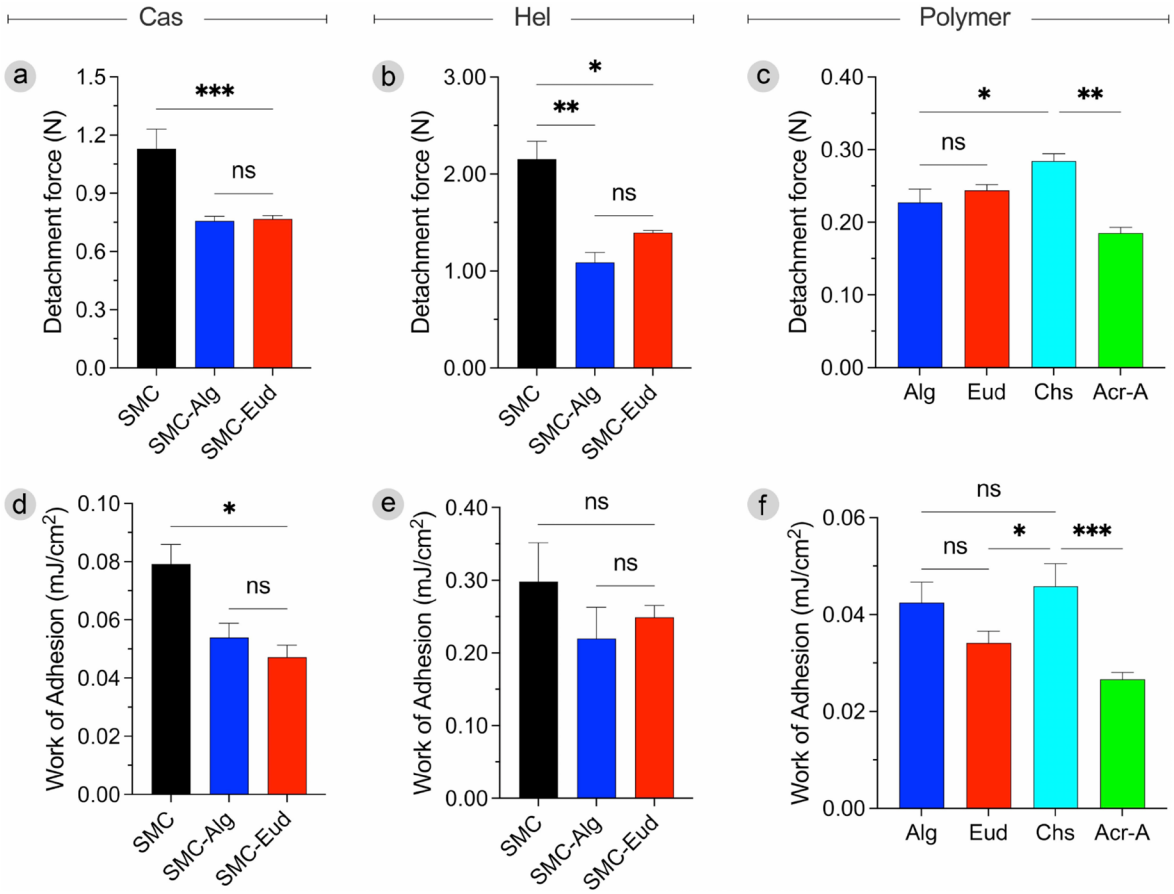

FIGURE 7 | Bioadhesive performance of uncoated and polymer-coated SMCs. (a) and (d) detachment force and work of adhesion for Cas type SMCs and coated variants. (b) and (e) detachment force and work of adhesion for Hel type SMCs and coated variants. (c) and (f) comparison of detachment force and work of adhesion for Alg, Eud, and also control polymers chitosan (Chs) and acrylic acid (Acr-A). Data is presented as mean ± SD ($n = 6$). *$p < 0.05$, **$p < 0.01$, and ***$p < 0.001$.

a detachment force value of approximately 2500 N/m^2 [55]. It should be noted that mucoadhesive force values obtained from texture analyzer measurements are highly dependent on experimental parameters, and therefore, direct comparison between different studies is often challenging due to the lack of standardized methodologies. The second parameter, work of adhesion, further supported these findings. Cas type SMCs exhibited a significantly higher work of adhesion (0.079 mJ/cm^2) than their polymer coated forms, Figure 7d. Hel type SMCs showed the highest value (0.298 mJ/cm^2), though this was not significantly different from the coated forms, Figure 7e. These measurements indicate that Hel type SMCs required approximately 3.8 times more energy to detach from mucin than Cas type. This is a critical feature because higher adhesion strength means stronger adhesion to biological tissues, which increases formulation residence time and potentially improves drug absorption [23].

The functional groups present on the sporopollenin shell are likely key contributors to the bioadhesive properties of SMCs. These groups enable multiple non-covalent interactions with mucin, a glycoprotein-rich component of mucus [23, 53]. The abundant hydroxyl (OH) groups on the SMC surface can engage in hydrogen bonding with complementary functional groups in mucin, such as hydroxyl, amine (NH_2), and carbonyl (C═O) groups. Additionally, the negatively charged carboxylate (COO^-) groups of sporopollenin may form electrostatic interactions with positively charged amine groups present in mucin under physiological pH conditions. Hydrophobic interactions may also play a role, facilitated by aromatic rings and phenolic carbonyl groups (C═O), as well as aliphatic C—H groups on the sporopollenin surface, which can interact with non-polar or aromatic residues in mucin. Together, these functional groups promote a combination of hydrogen bonding, electrostatic, and hydrophobic interactions that enhance the mucoadhesiveness of SMCs. The previous study has also linked the interaction and distribution of SMCs and human hepatocellular carcinoma cells to these same surface functionalities [56]. Similarly, another report attributes the mucoadhesive behavior of SMCs to the presence of functional groups capable of establishing hydrogen bonds with mucin [14], further supporting their role in enhancing adhesive performance. Moreover, Cas type SMCs exhibited a rugulate and relatively smoother surface architecture, whereas Hel type SMCs displayed a more complex perforate-striate texture. These distinct surface morphologies characteristic of their respective plant origins may contribute to differences in mucoadhesive behavior [14]. Variations in surface chemistry, topography, and roughness likely influence the extent of physical interaction with mucin, potentially accounting for the differential adhesion observed between Cas and Hel type SMCs, as seen in our previous work [25].

3.6 | Biocompatibility of SMCs

Regardless of whether they are synthetically produced or naturally derived, the compatibility of biomaterials with cells and tissues upon application to the body is of critical importance [6, 57]. In this study, the biocompatibility of SMCs produced from bee pollen pellets was evaluated using Vero cells, a kidney epithelial cell line, at concentrations ranging from 0.125 to 8 mg/mL. The SRB assay results demonstrated that both Cas and Hel-type SMCs did not induce cytotoxic effects in healthy cells, with GI_{50} values exceeding 700 μg/mL, indicating good biocompatibility. These findings are consistent with previous reports describing the biocompatibility of SMCs derived from various pollen sources. For instance, SMCs isolated from *Phoenix dactylifera* L. pollen were tested on Caco-2 cells at concentrations ranging from 0.1 to 200 mg/mL, resulting in cell viabilities between 91.6% and 87.4% [18]. In another study, the viability of primary microglial cells increased with increasing concentrations of *Helianthus annuus* derived SMCs after 24 and 48 h of culture, with cell viability increasing nearly fivefold at a concentration of 500 μg/mL [57]. Furthermore, various studies have reported that SMCs derived from different types of pollen, including sunflower, cattail, pine, dandelion, camellia, lotus, and poppy, did not exhibit significant cytotoxicity in dose-dependent studies conducted on both healthy and cancer cell lines [58–60]. Similarly, biocompatible behavior has been reported for SMCs isolated from *Lycopodium clavatum* [61]. Taken together, these results demonstrate the favorable biocompatibility of SMCs and support their safety for use in oral drug delivery applications.

4 | Conclusion

This study demonstrated that SMCs derived from Cas and Hel bee pollen possess promising potential as carriers for oral drug delivery, particularly for site-specific delivery to the gastrointestinal tract and colon. Both SMC types exhibited high drug loading capacities up to 36%, distinct morphological features, and mucoadhesive properties. Uncoated SMCs showed rapid drug release profiles dominated by Fickian diffusion, whereas Alg and Eud coatings significantly modified the release kinetics, achieving sustained and controlled drug delivery, particularly through super case II transport mechanisms. Importantly, Hel type SMCs displayed remarkable mucoadhesiveness and slower drug release compared with Cas type SMCs, likely due to their larger size and surface texture. Findings also demonstrated that SMCs derived from bee pollen did not adversely affect cell viability at the tested concentrations (0.125–8 mg/mL). These results underline the influence of both species-specific pollen morphology and polymeric coatings on the performance of SMC-based delivery systems.

Overall, the findings support the feasibility of using bee pollen-derived SMCs, either uncoated or polymer-modified, as natural, biocompatible, and tunable platforms for oral drug delivery. Their structural robustness, functional surface chemistry, and stability in environmental pH changes make them attractive candidates for further development in site-specific therapeutic applications.

Acknowledgments

The authors are grateful to the Foundation for Science and Technology (FCT, Portugal) for financial support by national funds FCT/MCTES to CIMO (UIDB/00690/2020 and UIDP/00690/2020), SusTEC (LA/P/0007/2021). Thanks to national funding, FCT for the Ph.D. research grant for Volkan Aylanc (2021.07764.BD) and Seymanur Ertosun (2021.08361.BD). Thanks to the NextGenerationEU recovery funds through the scope of Project BeeLand 10/C05-i03/2021.PPRR-C05-i03-I-00008.

Funding

This work was supported by Fundação para a Ciência e a Tecnologia, UIDB/00690/2020, UIDP/00690/2020, LA/P/0007/2021, 2021.07764.BD, 2021.08361.BD. NextGenerationEU, 10/C05-i03/2021.PPRR-C05-i03-I-00008.

Conflicts of Interest

The authors declare no conflicts of interest.

Data Availability Statement

The data that supports the findings of this study are available in the Supporting Information of this article.

References

1. C. S. Hu, S. L. Tang, C. H. Chiang, H. Hosseinkhani, P. Da Hong, and M. K. Yeh, "Characterization and Anti-Tumor Effects of Chondroitin Sulfate–Chitosan Nanoparticles Delivery System," *Journal of Nanoparticle Research* 16 (2014): 2672, https://doi.org/10.1007/s11051-014-2672-z.

2. W. He, H. Hosseinkhani, R. Mohammadinejad, et al., "Polymeric Nanoparticles for Therapy and Imaging," *Polymers for Advanced Technologies* 25 (2014): 1216–1225, https://doi.org/10.1002/pat.3381.

3. F. Mottaghitalab, M. Farokhi, M. A. Shokrgozar, F. Atyabi, and H. Hosseinkhani, "Silk Fibroin Nanoparticle as a Novel Drug Delivery System," *Journal of Controlled Release* 206 (2015): 161–176, https://doi.org/10.1016/j.jconrel.2015.03.020.

4. A. Kumari, S. K. Yadav, and S. C. Yadav, "Biodegradable Polymeric Nanoparticles Based Drug Delivery Systems," *Colloids and Surfaces. B, Biointerfaces* 75 (2010): 1–18, https://doi.org/10.1016/j.colsurfb.2009.09.001.

5. R. Cojocaru, O. Mannix, M. Capron, et al., "A Biological Nanofoam: The Wall of Coniferous Bisaccate Pollen," *Science Advances* 8 (2022): 892, https://doi.org/10.1126/sciadv.abd0892.

6. V. Aylanc, A. F. Peixoto, N. Vale, C. Freire, and M. Vilas-Boas, "Sporopollenin-Based Bio-Microcapsules as Green Carriers for Controlled Delivery of Pharmaceutical Drugs," *Applied Materials Today* 33 (2023): 101860, https://doi.org/10.1016/j.apmt.2023.101860.

7. N. M. Meligi, A. K. F. Dyab, and V. N. Paunov, "Sustained In Vitro and In Vivo Delivery of Metformin From Plant Pollen-Derived Composite Microcapsules," *Pharmaceutics* 13 (2021): 1048, https://doi.org/10.3390/pharmaceutics13071048.

8. C. Zhou, J. Deng, J. H. Tay, et al., "Multifunctional Material Building Blocks From Plant Pollen," *Annual Review of Chemical and Biomolecular Engineering* 15 (2024): 1–24, https://doi.org/10.1146/annurev-chembioeng-101121-085959.

9. L. Albano, A. Bento, V. G. Correia, and C. Silva Pereira, "The Chemistry of Sporopollenin Ektexine and Endexine Layers Isolated From Sunflower Pollen Through an Ionic Liquid-Mediated Process," *ACS Omega* 10 (2024): 411–421, https://doi.org/10.1021/acsomega.4c06524.

10. F. E. Atalay, A. A. Culum, H. Kaya, G. Gokturk, and E. Yigit, "Different Plant Sporopollenin Exine Capsules and Their Multifunctional Usage," *ACS Applied Bio Materials* 5 (2022): 1348–1360, https://doi.org/10.1021/acsabm.2c00071.

11. S. Ertosun, V. Aylanc, A. F. Peixoto, et al., "Structural Characterization of Microcapsules From Common Bee Pollen for the Development of Delivery Systems," *Journal of Polymers and the Environment* 33 (2024): 1171–1184, https://doi.org/10.1007/s10924-024-03478-0.

12. K. Stamatopoulos, V. Kafourou, H. K. Batchelor, and S. J. Konteles, "Sporopollenin Exine Microcapsules as Potential Intestinal Delivery System of Probiotics," *Small (Weinheim an Der Bergstrasse, Germany)* 17 (2021): 2004573, https://doi.org/10.1002/smll.202004573.

13. N. F. Taha, A. K. F. Dyab, L. H. Emara, and N. M. Meligi, "Microencapsulation of Diclofenac Sodium Into Natural *Lycopodium clavatum* Spores: In Vitro Release and Gastro-Ulcerogenic Evaluations," *Journal of Drug Delivery Science and Technology* 71 (2022): 103278, https://doi.org/10.1016/j.jddst.2022.103278.

14. A. Diego-Taboada, T. Sathyapalan, F. Courts, et al., "Spore Exines Increase Vitamin D Clinical Bioavailability by Mucoadhesion and Bile Triggered Release," *Journal of Controlled Release* 350 (2022): 244–255, https://doi.org/10.1016/j.jconrel.2022.08.017.

15. R. C. Mundargi, M. G. Potroz, S. Park, et al., "Lycopodium Spores: A Naturally Manufactured, Superrobust Biomaterial for Drug Delivery," *Advanced Functional Materials* 26 (2016): 487–497, https://doi.org/10.1002/adfm.201502322.

16. M. Raish, M. A. Kalam, A. Ahmad, et al., "Eudragit-Coated Sporopollenin Exine Microcapsules (SEMC) of *Phoenix dactylifera* L. of 5-Fluorouracil for Colon-Specific Drug Delivery," *Pharmaceutics* 13 (2021): 1921, https://doi.org/10.3390/pharmaceutics13111921.

17. A. S. Y. Mohammed, A. K. F. Dyab, F. Taha, and A. I. A. Abd El-Mageed, "Pollen-Derived Microcapsules for Aspirin Microencapsulation: In Vitro Release and Physico-Chemical Studies," *RSC Advances* 12 (2022): 22139–22149, https://doi.org/10.1039/D2RA02888C.

18. S. M. Alshehri, H. A. Al-Lohedan, A. A. Chaudhary, et al., "Delivery of Ibuprofen by Natural Macroporous Sporopollenin Exine Capsules Extracted From *Phoenix dactylifera* L," *European Journal of Pharmaceutical Sciences* 88 (2016): 158–165, https://doi.org/10.1016/j.ejps.2016.02.004.

19. S. V. Lale and H. S. Gill, "Pollen Grains as a Novel Microcarrier for Oral Delivery of Proteins," *International Journal of Pharmaceutics* 552 (2018): 352–359, https://doi.org/10.1016/j.ijpharm.2018.10.016.

20. V. Aylanc, A. F. Peixoto, L. Akyuz, N. Vale, C. Freire, and M. Vilas-Boas, "Natural Sporopollenin Microcarriers: Morphological Insights Into Their Functional Performance for Drug Encapsulation and Release," *International Journal of Biological Macromolecules* 314 (2025): 144384, https://doi.org/10.1016/j.ijbiomac.2025.144384.

21. R. C. Mundargi, E. L. Tan, J. Seo, and N. J. Cho, "Encapsulation and Controlled Release Formulations of 5-Fluorouracil From Natural *Lycopodium clavatum* Spores," *Journal of Industrial and Engineering Chemistry* 36 (2016): 102–108, https://doi.org/10.1016/j.jiec.2016.01.022.

22. C. E. Mora-Huertas, H. Fessi, and A. Elaissari, "Polymer-Based Nanocapsules for Drug Delivery," *International Journal of Pharmaceutics* 385 (2010): 113–142, https://doi.org/10.1016/j.ijpharm.2009.10.018.

23. V. V. Khutoryanskiy, "Advances in Mucoadhesion and Mucoadhesive Polymers," *Macromolecular Bioscience* 11 (2011): 748–764, https://doi.org/10.1002/mabi.201000388.

24. V. Aylanc, S. Ertosun, A. F. Peixoto, et al., "Development of Natural Sporopollenin Microcapsules: From Bee Pollen to Versatile Biomaterials," *Emergent Materials* 8 (2025): 3107–3122, https://doi.org/10.1007/s42247-025-01002-1.

25. V. Aylanc, A. F. Peixoto, R. C. Calhelha, et al., "A Clean Photochemical Pathway for Reconfiguring the Sporopollenin Biopolymer Into Sustainable Interfaces for Biocompatible Cellular Applications," *Applied Surface Science* 720 (2026): 165243, https://doi.org/10.1016/j.apsusc.2025.165243.

26. A. K. Prabhakar, M. G. Potroz, E. L. Tan, H. Jung, J. H. Park, and N. J. Cho, "Macromolecular Microencapsulation Using Pine Pollen: Loading Optimization and Controlled Release With Natural Materials," *ACS Applied Materials & Interfaces* 10 (2018): 28428–28439, https://doi.org/10.1021/acsami.8b09952.

27. A. S. de Carvalho, S. C. de Rezende, C. Caleja, et al., "β-Carotene Colouring Systems Based on Solid Lipid Particles Produced by Hot Melt Dispersion," *Food Control* 129 (2021): 108262, https://doi.org/10.1016/j.foodcont.2021.108262.

28. A. Brodkorb, L. Egger, M. Alminger, et al., "INFOGEST Static In Vitro Simulation of Gastrointestinal Food Digestion," *Nature Protocols* 14 (2019): 991–1014, https://doi.org/10.1038/s41596-018-0119-1.

29. J. N. Del Hierro, C. Cueva, A. Tamargo, et al., "In Vitro Colonic Fermentation of Saponin-Rich Extracts From Quinoa, Lentil, and Fenugreek. Effect on Sapogenins Yield and Human Gut Microbiota," *Journal of Agricultural and Food Chemistry* 68 (2020): 106–116, https://doi.org/10.1021/acs.jafc.9b05659.

30. H. Kranz, E. Yilmaz, G. A. Brazeau, and R. Bodmeier, "In Vitro and In Vivo Drug Release From a Novel In Situ Forming Drug Delivery System," *Pharmaceutical Research* 25 (2008): 1347–1354, https://doi.org/10.1007/s11095-007-9478-y.

31. M. L. Bruschi, ed., "Mathematical Models of Drug Release," in *Strategies to Modify the Drug Release From Pharmaceutical Systems* (Woodhead Publishing, 2015), 63–86, https://doi.org/10.1016/B978-0-08-100092-2.00005-9.

32. E. Cevher, M. A. M. Taha, M. Orlu, and A. Araman, "Evaluation of Mechanical and Mucoadhesive Properties of Clomiphene Citrate Gel Formulations Containing Carbomers and Their Thiolated Derivatives," *Drug Delivery* 15 (2008): 57–67, https://doi.org/10.1080/10717540701829234.

33. W. Voigt, "Sulforhodamine B Assay and Chemosensitivity," *Methods in Molecular Medicine* 110 (2005): 39–48, https://doi.org/10.1385/1-59259-869-2:039.

34. R. C. Mundargi, M. G. Potroz, S. Park, et al., "Natural Sunflower Pollen as a Drug Delivery Vehicle," *Small* 12 (2016): 1167–1173, https://doi.org/10.1002/smll.201500860.

35. R. C. Mundargi, N. B. Shelke, A. P. Rokhade, S. A. Patil, and T. M. Aminabhavi, "Formulation and In-Vitro Evaluation of Novel Starch-Based Tableted Microspheres for Controlled Release of Ampicillin," *Carbohydrate Polymers* 71 (2008): 42–53, https://doi.org/10.1016/j.carbpol.2007.05.013.

36. D. L. Melnikova, Z. F. Badrieva, M. A. Kostin, et al., "On Complex Formation Between 5-Fluorouracil and β-Cyclodextrin in Solution and in the Solid State: IR Markers and Detection of Short-Lived Complexes by Diffusion NMR," *Molecules* 25 (2020): 5706, https://doi.org/10.3390/molecules25235706.

37. G. Lawrie, I. Keen, B. Drew, et al., "Interactions Between Alginate and Chitosan Biopolymers Characterized Using FTIR and XPS," *Biomacromolecules* 8 (2007): 2533–2541, https://doi.org/10.1021/bm070014y.

38. N. Kumar, R. Aggarwal, and M. K. Chauhan, "Extended Levobunolol Release From Eudragit Nanoparticle-Laden Contact Lenses for Glaucoma Therapy," *Future Journal of Pharmaceutical Sciences* 6 (2020): 1–14, https://doi.org/10.1186/s43094-020-00128-9.

39. Y. Ding, C. Dou, S. Chang, et al., "Core–Shell Eudragit S100 Nanofibers Prepared via Triaxial Electrospinning to Provide a Colon-Targeted Extended Drug Release," *Polymers (Basel)* 12 (2020): 2034, https://doi.org/10.3390/polym12092034.

40. A. Lutzke, K. J. Morey, J. I. Medford, and M. J. Kipper, "Detailed Characterization of *Pinus ponderosa* Sporopollenin by Infrared

Spectroscopy," *Phytochemistry* 170 (2020): 112195, https://doi.org/10.1016/j.phytochem.2019.112195.

41. M. J. Uddin, S. Liyanage, N. Abidi, and H. S. Gill, "Physical and Biochemical Characterization of Chemically Treated Pollen Shells for Potential Use in Oral Delivery of Therapeutics," *Journal of Pharmaceutical Sciences* 107 (2018): 3047–3059, https://doi.org/10.1016/j.xphs.2018.07.028.

42. M. S. Hasanin, M. El-Sakhawy, H. Y. Ahmed, and S. Kamel, "Hydroxypropyl Methylcellulose/Graphene Oxide Composite as Drug Carrier System for 5-Fluorouracil," *Biotechnology Journal* 17 (2022): 2100183, https://doi.org/10.1002/biot.202100183.

43. M. Samy, H. M. Abdallah, H. M. Awad, and M. M. H. Ayoub, "Preparation, Characterization and In Vitro Biological Activity of 5-Fluorouracil Loaded Onto Poly (D, L-Lactic-Co-Glycolic Acid) Nanoparticles," *Polymer Bulletin* 80 (2023): 6197–6219, https://doi.org/10.1007/s00289-022-04308-w.

44. P. dos Santos Araújo, G. B. Belini, G. P. Mambrini, F. M. Yamaji, and W. R. Waldman, "Thermal Degradation of Calcium and Sodium Alginate: A Greener Synthesis Towards Calcium Oxide Micro/Nanoparticles," *International Journal of Biological Macromolecules* 140 (2019): 749–760, https://doi.org/10.1016/j.ijbiomac.2019.08.103.

45. C. J. Perecin, X. P. M. Gratens, V. A. Chitta, et al., "Synthesis and Characterization of Magnetic Composite Theragnostics by Nano Spray Drying," *Materials* 15 (2022): 1755, https://doi.org/10.3390/ma15051755.

46. L. Akyuz, I. Sargin, M. Kaya, T. Ceter, and I. Akata, "A New Pollen-Derived Microcarrier for Pantoprazole Delivery," *Materials Science and Engineering: C* 71 (2017): 937–942, https://doi.org/10.1016/j.msec.2016.11.009.

47. M. J. Uddin, N. Abidi, J. Warzywoda, and H. S. Gill, "Investigation of the Fate of Proteins and Hydrophilicity/Hydrophobicity of *Lycopodium clavatum* Spores After Organic Solvent-Base-Acid Treatment," *ACS Applied Materials & Interfaces* 11 (2019): 20628–20641, https://doi.org/10.1021/acsami.9b03040.

48. J. M. Lakkis, "Encapsulation and Controlled Release Applications in Confectionery and Oral Care Products," in *Encapsulation and Controlled Release Technologies in Food Systems* (John Wiley & Sons, Ltd, 2016), 236–288, https://doi.org/10.1002/9781118946893.ch9.

49. J. Jablan and M. Jug, "Development of Eudragit S100 Based pH-Responsive Microspheres of Zaleplon by Spray-Drying: Tailoring the Drug Release Properties," *Powder Technology* 283 (2015): 334–343, https://doi.org/10.1016/j.powtec.2015.05.045.

50. F. Abedini, M. Ebrahimi, A. H. Roozbehani, A. J. Domb, and H. Hosseinkhani, "Overview on Natural Hydrophilic Polysaccharide Polymers in Drug Delivery," *Polymers for Advanced Technologies* 29 (2018): 2564–2573, https://doi.org/10.1002/pat.4375.

51. M. Micutz, V. Circu, M. Ilis, and T. Staicu, "Novel Gemini Surfactant for Binding Eu(III)-Polyoxometalate Into Hydrogels and Polymer Latexes," *Gels* 8 (2022): 786, https://doi.org/10.3390/gels8120786.

52. J. M. Budinčić, L. Petrović, L. Đekić, et al., "Study of Vitamin E Microencapsulation and Controlled Release From Chitosan/Sodium Lauryl Ether Sulfate Microcapsules," *Carbohydrate Polymers* 251 (2021): 116988, https://doi.org/10.1016/j.carbpol.2020.116988.

53. R. Shaikh, T. Raj Singh, M. Garland, A. Woolfson, and R. Donnelly, "Mucoadhesive Drug Delivery Systems," *Journal of Pharmacy & Bioallied Sciences* 3 (2011): 89–100, https://doi.org/10.4103/0975-7406.76478.

54. E. Baloglu, Z. A. Senyigit, S. Y. Karavana, et al., "In Vitro Evaluation of Mucoadhesive Vaginal Tablets of Antifungal Drugs Prepared With Thiolated Polymer and Development of a New Dissolution Technique for Vaginal Formulations," *Chemical & Pharmaceutical Bulletin (Tokyo)* 59 (2011): 952–958, https://doi.org/10.1248/cpb.59.952.

55. G. Di Prima, C. La Mantia, G. Tranchida, et al., "Mucoadhesive Buccal Patches Containing Resveratrol and/or Erythromycin-Loaded Lipid Microparticles as a Potential Targeted Strategy for the Prevention and Management of MRONJ in Patients Undergoing Oral Surgery," *Antibiotics* 15 (2026): 151, https://doi.org/10.3390/antibiotics15020151.

56. E. L. Tan, M. G. Potroz, G. Ferracci, L. Wang, J. A. Jackman, and N. J. Cho, "Hydrophobic to Superhydrophilic Tuning of Multifunctional Sporopollenin for Microcapsule and Bio-Composite Applications," *Applied Materials Today* 18 (2020): 100525, https://doi.org/10.1016/j.apmt.2019.100525.

57. M. Li, B. Hu, Z. Wu, et al., "Sporopollenin Exine Capsules Modulate the Function of Microglial Cells," *Biomaterials Science* 12 (2024): 710–724, https://doi.org/10.1039/D3BM01154B.

58. T. Maric, M. Z. M. Nasir, N. F. Rosli, et al., "Microrobots Derived From Variety Plant Pollen Grains for Efficient Environmental Clean up and as an Anti-Cancer Drug Carrier," *Advanced Functional Materials* 30 (2020): 2000112, https://doi.org/10.1002/adfm.202000112.

59. B. Khann, D. Polpanich, P. Opaprakasit, Y. Wongngam, K. Thananukul, and C. Kaewsaneha, "Fabrication of Sacha Inchi Oil-Loaded Microcapsules Employing Natural-Templated *Lycopodium clavatum* Spores and Their Pressure-Stimuli Release Behavior," *ACS Omega* 8 (2023): 20937–20948, https://doi.org/10.1021/acsomega.3c01698.

60. S. Zhou, D. Wu, Z. Xu, and Q. Jiang, "Sporopollenin Exine Capsules With Polypeptide Multilayer Films Promoting Cell Adhesion," *Chemical Engineering Journal* 475 (2023): 145607, https://doi.org/10.1016/j.cej.2023.145607.

61. A. K. F. Dyab, M. A. Mohamed, N. M. Meligi, and S. K. Mohamed, "Encapsulation of Erythromycin and Bacitracin Antibiotics Into Natural Sporopollenin Microcapsules: Antibacterial, Cytotoxicity, In Vitro and In Vivo Release Studies for Enhanced Bioavailability," *RSC Advances* 8 (2018): 33432–33444, https://doi.org/10.1039/C8RA05499A.

Supporting Information

Additional supporting information can be found online in the Supporting Information section. **Table S1:** Preparation of simulated digestion fluids stock solutions: simulated gastric fluid (SGF) and intestinal fluid (SIF) stock solutions. The final volume for each digestive fluid is 500 mL at a concentration of 1.25 × [1].